Transport of thermal-energy ionospheric oxygen (O^+) ions between the ionosphere and the plasma sheet and ring current at quiet times preceding magnetic storms

Andrew W. Yau,[1] Andrew Howarth,[1] W. K. Peterson,[2] and Takumi Abe[3]

Received 4 April 2012; revised 21 May 2012; accepted 1 June 2012; published 20 July 2012.

[1] The presence of energetic O^+ ions in the ring current at the onset of a magnetic storm prompts the question of the possible role of "in-transit" ionospheric O^+ ions between the ionosphere and the plasma sheet and ring current in the quiet periods immediately preceding the main phase of a magnetic storm. Thermal-energy O^+ ions are often observed in the quiet time high-altitude (>7000 km) polar ionosphere on Akebono, at temperatures of ~0.2–0.3 eV and flow velocities of a few km/s. In this paper, we use single-particle trajectory simulation to study the transport of these ions in the periods preceding a number of large magnetic storms (Dst < −100 nT). Our simulation shows that due to centrifugal ion acceleration at higher altitudes (above ~3 R_E altitude), about 10–20% of polar wind and other low-energy O^+ ions reaches the plasma sheet during such periods; the actual percentage is a factor of ~3 larger in the dusk sector on average compared with the dawn sector and dependent on the IMF and the O^+ ion temperature. This provides a low but non-negligible flux of O^+ ions between the ionosphere and the plasma sheet and ring current, which is believed to constitute a significant "in-transit" oxygen ion population over a period of a few (~4) hours preceding a magnetic storm. Such a population could explain the presence of energetic O^+ ions at the onset of the main phase of the storm, when the heavy ions could potentially modify the evolution of the ring current.

Citation: Yau, A. W., A. Howarth, W. K. Peterson, and T. Abe (2012), Transport of thermal-energy ionospheric oxygen (O^+) ions between the ionosphere and the plasma sheet and ring current at quiet times preceding magnetic storms, *J. Geophys. Res.*, *117*, A07215, doi:10.1029/2012JA017803.

1. Introduction

[2] The plasma in the ring current is believed to come primarily from the plasma sheet, which in turn originates from the solar wind and the ionosphere; see for example the comprehensive review of *Hultqvist et al.* [1999] on the sources and losses of plasma in different magnetospheric regions. Within the ring current plasma, the energetic O^+ ion population is believed to originate from the ionosphere, and to play an important role in the particle and magnetic field pressure distributions during a geomagnetic storm [*Fok et al.*, 2001; *Jordanova*, 2003; *Zaharia et al.*, 2006]. Since the latter are an integral part of the large-scale magnetospheric current system, the nature of energization and transport of the seed O^+ populations in the ionosphere is believed to be an important part of the ring current dynamics.

[3] The outflow rate of energetic (>10 eV) upflowing ionospheric O^+ ions is strongly dependent on both geomagnetic and solar activity levels [*Yau et al.*, 1985]. Using data from the DE-1 energetic ion composition spectrometer (EICS) between 16,000 and 24,000 km altitude, *Yau et al.* [1988] parameterized the observed *hemispherical* flux F of >10-eV O^+ ions as a function of the solar radio flux and K_P indices. Explicitly, $F(K_P, F_{10.7}) = 5 \times 10^{24} \exp[0.01 (F_{10.7} - 100)] \exp(0.50\ K_P)$, and the hemispherical flux ranges from 3.7×10^{24} ions s^{-1} at $K_P = 0$, $F_{10.7} = 70$, to 2×10^{26} ions s^{-1} at $K_P = 9$, $F_{10.7} = 250$, corresponding to a range of 0.2–10 kg/s in O^+ mass outflow rate over the two hemispheres.

[4] The thermal plasma density in the polar ionosphere is found to exhibit a significant variation with seasons, and to transition from an exponential altitude dependence at low altitude to a power law relationship at high altitude up to at least ~10,000 km, i.e., $n_e = n_1 \exp(-z/h) + n_2 r^{-\alpha}$, where n_e is the median electron density, the coefficients n_1, n_2, h and α are a function of the season, invariant latitude and local time, and the power law and exponential terms equal each other at the transition height (H_T) [*Kitamura et al.*, 2009]. Near solar maximum, the transition height varies from

[1]Department of Physics and Astronomy, University of Calgary, Calgary, Alberta, Canada.
[2]Laboratory of Atmospheric and Space Physics, University of Colorado Boulder, Boulder, Colorado, USA.
[3]Institute of Space and Astronautical Science, Japan Aerospace Exploration Agency, Sagamihara, Japan.

Corresponding author: A. W. Yau, Department of Physics and Astronomy, University of Calgary, 2500 University Dr. NW, Calgary, AB T2N1N4, Canada. (yau@phys.ucalgary.ca)

0148-0227/12/2012JA017803

~1500 km to ~4000 km and the plasma density (n_e) ranges from about 20 to 10^2 cm^{-3} above 6000 km altitude at equinox.

[5] As discussed in *Chappell et al.* [1987] and *Yau and Andre* [1997], the polar wind constitutes a dominant component of the thermal plasma in the polar ionosphere, and it exhibits several "non-classical" features at high altitude, which are attributed to a number of ion acceleration mechanisms associated with strong ionospheric convection in regions of large magnetic field curvatures, enhanced electron and ion temperatures, and escaping atmospheric photoelectrons [*Yau et al.*, 2007]. At Akebono altitudes (<10,000 km), the observed polar wind is comprised mainly of H^+, He^+ and O^+ ions, and electrons. The ions have an averaged ion temperature of ~0.2–0.3 eV [*Drakou et al.*, 1997], a day-night asymmetry in ion velocity (larger averaged velocity on the dayside), and a rate of increase in ion velocity with altitude that correlates strongly with electron temperature and varies with solar activity level [*Abe et al.*, 2004]. At a given altitude, the polar wind velocity is highly variable, and is on average largest for H^+ and smallest for O^+.

[6] O^+ ions often constitute a significant and at times dominant component of the thermal ion population, the observed O^+/H^+ ratio being in the range of 0.1–0.5 near solar maximum [*Yau et al.*, 1991] and in a lower range near solar minimum [*Cully et al.*, 2003a]. Thus, the observed O^+ polar wind at Akebono altitudes may be characterized by a cold, drifting plasma with a temperature of ~0.2–0.3 eV, a drift velocity of ~2–4 km/s and a seasonally dependent density of a few to ~30 cm^{-3} near solar maximum, and it represents a non-negligible supply of escaping low-energy O^+ ions; note, however, that observationally it is not always possible to unambiguously separate polar wind O^+ ions from other low-energy ion populations, such as a low-energy "cleft ion fountain" ion that has convected into a polar wind flux tube.

[7] *Peterson et al.* [2008] estimated the escaping hemispherical O^+ ion flux and characteristic energy at ~6000 km at magnetically quiet times, by including both the energetic (0.015–17 keV) ion data from the torodial ion mass angle spectrograph (TIMAS) [*Lennartsson et al.*, 2004] and the thermal (0–50 eV) ion data from the thermal ion dynamics experiment (TIDE) [*Su et al.*, 1998] on Polar, and assuming uniform thermal ion flux throughout the auroral zone and polar cap and a characteristic energy of 1 eV in the thermal component. Near solar minimum, the estimated flux was ~4.6×10^{24} in the auroral region and 6.2×10^{24} ions s^{-1} in the polar cap. The thermal component was estimated to constitute as much as ~63 and 99% in the two regions. As discussed in *Huddleston et al.* [2005] using the Polar TIDE data, observed low-energy ion fluxes are often subject to large uncertainties due to spacecraft potential effects. However, as demonstrated by *Watanabe et al.* [1992] in the Akebono data for example, it is sometimes possible to reduce such uncertainties considerably by correcting for the "hidden" component in the ion velocity distribution due to positive spacecraft potential.

[8] The escape velocity v_e of a particle in the exosphere is determined by the kinetic energy required to overcome the Earth's gravitational potential and is given by $v_e = (2\, g_0\, R_E^2/r)^{1/2}$, where g_0 is the acceleration due to gravity at the Earth surface, R_E is the Earth radius, and r is the radial distance of the particle. Thus, v_e is ~11 km/s at the exobase (500 km altitude) and ~8 km/s at 1 R_E altitude independent of ion mass species. In comparison, the typical velocity of a polar wind O^+ ion is much smaller (~2–4 km/s) near 1 R_E altitude, while the velocity of a cleft ion fountain O^+ ion with a drift energy of 10–20 eV is larger (10–15 km/s). However, in the context of polar wind plasma transport, it is important to recognize that the escape velocity corresponds to the velocity that an ion needs to reach an infinite distance from Earth in the absence of any acceleration. The minimum velocity required for the ion to reach the magnetosphere is often smaller, since the distance between the ionosphere and the magnetosphere is not infinite, and as noted above a number of acceleration mechanisms exist between the two.

[9] To assess the possibility of the oxygen polar wind being a potential source of plasma sheet and ring current plasma, it is instructive to compare the observed O^+ density and temperature and the corresponding escaping fraction due to thermal Jeans escape at 500, 7000, and 50,500 km, which correspond to the exobase, the altitude of Akebono data in the present study, and the Polar apogee and the highest altitude of available polar wind data, respectively. The fraction of escaping particles in a drifting Maxwellian is given by $f_{esc} = 1/2\{1 - [1 - \exp(-(v_e - v_d)^2/v_t^2)]^{1/2}$, where v_d and v_t are the particle vertical drift and thermal velocity, respectively; $v_d < v_e$, $v_t = (kT/m)^{1/2}$, and m and T are particle mass and temperature. At the exobase, where the O^+ density is typically <10^5 cm^{-3} and the temperature is typically 0.1 eV, the fraction of escaping O^+ ions is obviously negligible (<10^{-80}). At Akebono altitude where the temperature is ~0.2 to 0.3 eV and the parallel velocity is ~2–4 km/s, as noted above, the fraction of escaping ions is much less negligible although it remains much smaller than unity ($\leq 2 \times 10^{-6}$). More important, the solar-maximum density of ≤30 cm^{-3} is clearly many orders of magnitude larger than the escaping density at the exobase, and reflects the effect of the overall polar wind acceleration in "lifting" a significant fraction of the plasma between the two altitudes.

[10] Likewise, at Polar apogee, the observed O^+ density near solar minimum (0.05 cm^{-3}) [*Su et al.*, 1998] is about 3 orders of magnitude larger than the escaping ion density ($\leq 6 \times 10^{-5}$ cm^{-3}) at Akebono altitude; the corresponding density near solar maximum is expected to be larger. The observed temperature (7.5 eV) and drift velocity (16.8 km/s) are also much larger, and imply the occurrence of additional acceleration that is required to lift a sufficient fraction of the ions from the Akebono altitude to the Polar apogee.

[11] *Cully et al.* [2003a] compared the observed magnitudes and $F_{10.7}$ and K_P dependences of low-energy H^+ and O^+ ion outflows on Akebono with those of energetic ion outflows on DE-1 and Polar, and found that the low-energy H^+ flow at Akebono altitude was entirely sufficient to account for the higher-energy flows at higher altitudes. In contrast, the low-energy O^+ flow could account for only a small fraction of the higher-energy flows at higher altitudes. In addition, both H^+ and O^+ outflow rates exhibited a strong correlation with the solar wind kinetic pressure, solar wind electric field, and interplanetary magnetic field (IMF) variability (δB_{IMF}) in the preceding hour; similar correlations between upwelling ions and IMF were observed on DE-1 [*Pollock et al.*, 1990]. In particular, the rates exhibited a

strong correlation with solar wind density and anti-correlation with solar wind velocity, independent of K_P.

[12] Previous authors have used a number of single-particle trajectory tracing models to investigate the transport of ionospheric ions of various energies in the magnetosphere. Using a simple 2-dimensional model, *Cladis* [1986] demonstrated the importance of centrifugal ion acceleration in regions of curved or changing magnetic field. *Delcourt et al.* [1989, 1993, 1994] used both the guiding center and full equations of motion to study the 3-dimensional dynamics of auroral, polar cap, cusp and H^+ polar wind ions in different magnetospheric regions including the magnetotail. The H^+ polar wind was found to constitute a significant supply of H^+ ions to the plasma sheet particularly under magnetically quiet times, when the ions can reach further down tail under the influence of a weaker convection electric field and interact non-adiabatically in the plasma sheet.

[13] *Cully et al.* [2003b] used the guiding center equations to address the question of auroral substorm trigger and the supply of various types of low-energy ions to the central plasma sheet under both northward and southward IMF conditions, including both light (H^+) and heavy (O^+) polar wind and "cleft ion fountain" ions. It was found that a drastic northward turning of the IMF results in a reduced supply of O^+ ions to the near-tail region of the plasma sheet, where substorm onset is thought to originate. In addition, the low-energy O^+ ions often traverse along a field line for a long duration compared with the duration of magnetospheric reconfiguration during disturbed periods.

[14] In a follow-on study, *Howarth and Yau* [2008] examined the influence of the IMF and convection electric field on the trajectories and destinations of polar wind and other low-energy ions observed on Akebono in the case of steady IMF and ionospheric convection. Ions were found to preferentially feed the dusk sector of the plasma sheet over the dawn sector when the IMF is duskward ($B_y > 0$), and to be more evenly distributed between the two sectors when the IMF is dawnward. It was also found that a larger percentage of O^+ ions originating from the noon or dusk sectors of the polar cap reaches the magnetosphere and beyond compared with ions from the dawn or midnight sectors, due to the increased centrifugal acceleration associated with the larger magnetic field curvature near noon and the larger convection electric field in the dusk sector. In addition, the O^+ outflow rate to both the plasma sheet and the magnetotail was found to correlate strongly with the ion temperature.

[15] In a similar study, *Ebihara et al.* [2006] simulated the destination of suprathermal energy (14–209 eV) ionospheric O^+ ions observed on Akebono. This simulation used the full equation of motion and an empirical model of ion flux, which is based on K_P and the sunspot number and derived from Akebono suprathermal ion mass spectrometer (SMS) data. It assumed a source altitude of 1 R_E and time-independent external magnetic and convection electric fields using the Tsyganenko T89c [*Tsyganenko*, 1989] and Weimer W2K [*Weimer*, 2001] models. Under an active-time magnetic field and "mid-strength" convection electric field, the majority of O^+ ions that were above escape energy at the source altitude were found to reach the ring current, and only a very small fraction reached the magnetopause or the distant tail and the atmosphere. In comparison, under quiet time conditions, the fraction of suprathermal ions reaching the ring current was a factor of 3 smaller, and the fractions reaching the magnetopause and the distant tail were a factor of 2 and 200 larger, respectively. In a subsequent case study of two geomagnetic storms using the same simulation code, *Kitamura et al.* [2010] found that some of the low-energy (a few eV) cleft ion fountain O^+ ions could also be transported to the ring current region during the storms.

[16] *Huddleston et al.* [2005] extended the simulation code of *Delcourt et al.* [1993] to compute the full trajectories of H^+ and He^+ polar wind (0–3 eV) and cleft ion fountain (10–20 eV) ions, as well as O^+ cleft ion fountain and H^+ and O^+ auroral (500 eV) ions. A Volland electric field model with a Heelis correction was used in combination with ion measurements from the Polar TIDE instrument, and detailed trajectories were calculated for quiet and moderate levels of magnetic activity. An H^+ polar wind ion originating from the Polar perigee (5000 km) at auroral latitudes was often found to lose its kinetic energy initially but gradually gain energy at higher altitude due to "centrifugal acceleration," as it experienced magnetic curvature drift through the convection electric field potential while convecting across the polar cap into the magnetospheric lobes. Thereafter, as the ion traversed the highly curved magnetic field in the neutral sheet, it was further and abruptly accelerated to "plasma sheet" energies of hundreds of eV. Thus, polar wind H^+ ions originating from or below auroral latitudes were interpreted as an important source of plasma sheet H^+ ions. In the case of the cleft ion fountain and auroral ions, the trajectories of different ion species originating from the same source location were found to deviate from each other, with the heaviest ion species (O^+) reaching least down tail and the lightest ion species (H^+) farthest down tail.

[17] In general, a geomagnetic storm has three phases: initial, main and recovery, and it can be classified as recurrent or non-recurrent. Recurrent storms, which occur most frequently in the declining phase of a solar cycle once every 27-day solar rotation, are believed to be triggered by a region of high solar wind pressure formed by the interaction of low- and high-speed co-rotating solar wind streams. Non-recurrent geomagnetic storms, which occur most frequently near solar maximum, are believed to be triggered by a fast coronal mass ejection (CME) and the accompanying interplanetary shock wave. In both cases, a magnetic storm is often associated with the southward turning of the IMF, which results in an enhanced coupling between the IMF and the Earth's internal magnetic field; the enhanced coupling in turn intensifies the westward ring current and the induced southward magnetic field at the equator – and decreases the disturbance-storm time index (Dst) in the main phase of a storm.

[18] The initial phase, or storm sudden commencement (SSC), of a geomagnetic storm typically lasts 2 h or longer and is characterized by an increase in the Dst index by up to about 50 nT, resulting from the compression of the magnetosphere due to the arrival of a CME, interplanetary shock, and/or sudden solar wind plasma pressure enhancement; not all geomagnetic storms have an initial phase, and not all SSC are followed by a geomagnetic storm. The main phase typically lasts several hours and is characterized by a decrease in Dst to a minimum value, which results from the intensification of the ring current and induced magnetic field at the equator, as noted above; storms with minimum Dst values of

less than −50, −100, and −250 nT are customarily referred to as "moderate," "large," and "super" storms, respectively. The recovery phase typically lasts up to a day or longer and is characterized by the gradual increase in Dst to the pre-storm value, due to the gradual decay of the ring current resulting from the loss of the current-carrying energetic charged particles to charge exchange and other mechanisms.

[19] In this paper, we extend the simulation model in *Howarth and Yau* [2008] to the case of time-dependent magnetic and convection electric field, to study the transport of thermal-energy polar wind O^+ ions in the quiet time periods immediately preceding a number of large magnetic storms. Our focus is on the time period immediately preceding the onset of the main phase of a storm: this onset is identified as the time when Dst started to turn negative or to decrease sharply in the case of a storm with and without an initial phase, respectively.

[20] The organization of this paper is as follows. Section 2 briefly describes the trajectory tracing model. Section 3 presents the simulated trajectories and magnetospheric destinations of quiet time polar wind O^+ ions preceding a number of magnetic storm events. Section 4 discusses the feeding of these ions to the plasma sheet immediately preceding and at storm onset and the resulting effects on the plasma sheet and the ring current in the main phase of the storm.

2. Particle Trajectory Simulation

[21] The aim of the present simulation study is to determine the trajectories of polar wind O^+ ions in the high-altitude polar ionosphere in the quiet time period preceding a magnetic storm, in order to determine their percentage (if any) and final energy and destination in the magnetosphere, and their overall possible effects on the plasma sheet and ring current. A total of five magnetic storms in 2000–2005 were selected for analysis; this period spanned the maximum and the early declining phase of Solar Cycle 23 (SC 23). In each case, simulation was performed for ions from different invariant latitude and MLT locations covering both the polar cap and the auroral zone, and starting at different initial velocities and different times preceding storm onset.

2.1. Simulation Model

[22] The simulation model was adapted from *Cully et al.* [2003b] and *Howarth and Yau* [2008], and the simulation region encompasses the region of X_{GSM} = +10 to −70 R_E, Y_{GSM} = −25 to +25 R_E, and Z_{GSM} = −30 to +30 R_E. Starting at its source location $\mathbf{R}_0$ ($\equiv\mathbf{R}(t = t_0)$) and initial velocity $\mathbf{v}_0$ ($\equiv\mathbf{v}(t = t_0)$), the final destination of a particle can be determined by solving the full equation of motion:

$$\frac{d\vec{\mathrm{v}}}{dt} = \frac{q}{m}\left(\vec{E} + \vec{\mathrm{v}} \times \vec{B}\right) + \vec{G} \quad ; \quad \vec{G} = \frac{G_M M_E}{R^3}\ \vec{r} \qquad (1)$$

In equation (1), q is the charge, m is the mass, and r is the radial distance of the particle from the Earth center; E is the electric field, B is the magnetic field, and G is the gravitational acceleration; G_M and M_E are the Earth's gravitational constant and mass, respectively. However, it is often computationally time-consuming to solve equation (1) for a large number of single particles due to the large amount of computations required to follow the gyromotion of each particle as it traverses the magnetosphere. Under adiabatic conditions, where the electric and magnetic fields do not vary significantly over a gyroperiod or gyroradius, it is sufficient to use the first-order guiding center equations of motion [*Northrop*, 1963]:

$$\frac{d\mathrm{v}_{/\!/}}{dt} = G_\parallel + \frac{q}{m}E_\parallel - \frac{\mu}{m}\nabla_\parallel B + \vec{\mathrm{v}}_{\vec{E}\times\vec{B}} \cdot \frac{d\hat{B}}{dt} \qquad (2)$$

$$\vec{\mathrm{v}}_\perp = \frac{\vec{E}\times\vec{B}}{B^2} + \frac{\mu}{qB^2}\vec{B}\times\nabla B + \frac{m}{qB^2}\vec{G}\times\vec{B} - \frac{m}{qB^2}\left[\mathrm{v}_\parallel \frac{d\hat{B}}{dt} + \frac{d\vec{\mathrm{v}}_{\vec{E}\times\vec{B}}}{dt}\right] \times \vec{B} \qquad (3)$$

In equations (2) and (3), μ is the magnetic moment, the last term in (2) is the centrifugal acceleration term first discussed by *Cladis* [1986], and the time derivatives are convective derivatives and they depend on both time and space, i.e.

$$\frac{d}{dt}A = \left[\frac{\partial}{\partial t} + \mathrm{v}_\parallel\nabla_\parallel + \left(\vec{\mathrm{v}}_{\vec{E}\times\vec{B}}\cdot\nabla\right)\right]\ A \qquad (4)$$

In order to trace the trajectories of a statistically significant number of particles, the guiding center equations (2) and (3) were used in the present study, except in the non-adiabatic regions of the plasma sheet and ring current in Figures 3a–3c where the full equation (1) was used instead; in these regions, the ratio of the minimum field-line curvature encountered by an ion to the maximum ion gyroradius in a time step is expected to be small (<10). A fifth-order Runge-Kutta integration method was used to obtain the numerical solution in both cases.

[23] The magnetic field was determined from a superposition of the Internal Geomagnetic Reference Field (IGRF) [*Finlay, et al.*, 2010], and the Tsyganenko 1996 (T96) external magnetic field model [*Tsyganenko*, 1995; *Tsyganenko and Stern*, 1996], which is parameterized by the Dst index and the Earth's dipole tilt angle, as well as instantaneous values of the solar wind dynamic pressure P_{dyn} and IMF B_Y and B_Z; the latter values were derived by time-shifting the solar wind measurements on ACE based on the satellite position (X_{GSM}) and measured solar wind velocity. The T96 model is most accurate within recommended intervals of these parameters ($0.5 < P_{dyn} < 10$ nPa; $-100 <$ Dst < 20 nT; and $-10 < B_Y, B_Z < 10$ nT), where satellite measurement data are more extensive. The model is expected to be more approximate or to be unrealistic in large magnetic storms in which the minimum Dst is beyond the recommended interval; its effect on the present study will be discussed in section 4.

[24] The electric field was determined in two steps. The electric field potential at the ionospheric level was first inferred from SuperDARN ion convection velocity data, and from the Applied Physics Lab statistical model [*Ruohoniemi and Greenwald*, 1996; *Shepherd and Ruohoniemi*, 2000] in the case of data gaps. The potential distribution was then mapped along the field lines to simulate the electric field at higher altitudes, by assuming the absence of parallel electric field (i.e., $E_{/\!/} = 0$), everywhere in the magnetosphere. This assumption is justified [*Howarth and Yau*, 2008] since the ambipolar electric field in the polar wind is typically less

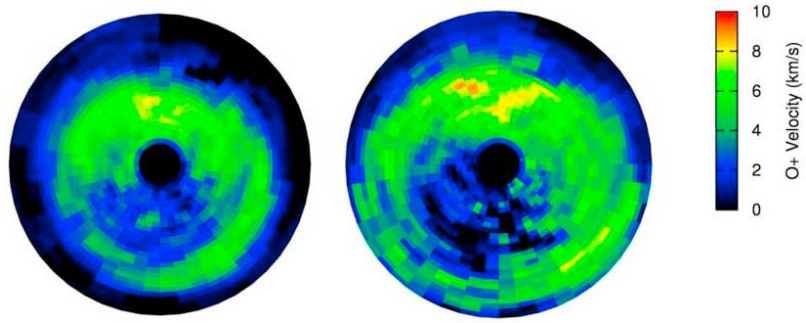

Figure 1. Averaged polar wind O^+ velocity between 6000 and 8000 km altitude observed on Akebono near solar maximum, for low and high K_P conditions: (left) $K_P < 4$ and (right) $K_P \geq 4$; adapted from *Abe et al.* [2004].

than 10^{-7} V m^{-1} and much smaller than the perpendicular convection electric field $E_\perp$ in the simulation region (>7000 km altitude).

[25] To expedite the computation, a non-uniformly spaced grid of 101 × 101 × 101 grid points was used in which the grid spacing varied with the radial distance at a grid point from a minimum of ~1/3 R_E, and both the electric and magnetic fields at each grid point were pre-computed and updated every 10 min in response to the changing solar wind dynamic pressure and IMF. During the particle tracing, the E and B values at any position and time were obtained from the corresponding values at the nearest grid points in the nearest updates using linear interpolation in time and in space.

2.2. Particle Trajectories and Destinations

[26] Starting at 4 h or more before the onset in each storm, a total of 10,000 ions were "launched" from an altitude of 7000 km every 10 min. To ensure a statistically representative sampling of the large region of phase space, a Monte Carlo technique was used to randomly select the initial position (between 70° and 86° invariant and at all MLT) and velocity for each ion.

[27] The Monte Carlo position selection assumed uniform ion density at all invariant latitudes above 70° and all MLT. The random velocity selection assumed a drifting Maxwellian velocity distribution with an ion temperature of 0.25 eV, a perpendicular velocity derived from the SuperDARN convection electric field data, and a parallel drift velocity derived from the observed polar wind O^+ velocity distribution between 6000 and 8000 km altitude [*Abe et al.*, 2004] as shown in Figure 1, as a function of the selected invariant latitude and MLT location.

[28] The trajectory of each ion was followed until it reached one of 9 possible final destinations, and the initial and final position and velocity of each ion were captured for analysis. An ion was identified as "trapped" in the *atmosphere* if it was gravitationally trapped, descended below 600 km, or was below 1 R_E altitude after two hours. An untrapped ion could convect to the *dayside* equatorial plane; reach the *magnetopause* or its vicinity where the field lines did not connect back to the ionosphere in the T96 model; flow to the *distant tail* beyond $X_{GSM} = -66\ R_E$; cross the Plasma Sheet Boundary Layer (PSBL) tail-ward of $X_{GSM} = -15\ R_E$ into the *dawn tail* or *dusk tail*; cross the PSBL earthward of $-15\ R_E$ into the *dawn plasma sheet* or *dusk plasma sheet*; or flow out of the simulation region altogether.

[29] Following *Howarth and Yau* [2008], the PSBL was defined as a function of the dipole tilt angle, and serves as the cutoff where the ions begin to experience non-adiabatic energization in the plasma sheet. In test simulation runs, the guiding center solution for none of the ions was found to deviate appreciably from the full solution at the cutoff, indicating that the ions remained adiabatic. Also, only a small fraction of a percent of the ions was found to flow out of the simulation region. This fraction of ions is excluded from the analysis below, which will focus on the other 8 ion destinations, including the atmosphere for the trapped ions and the 7 magnetospheric regions for the non-trapped ions: the dayside, magnetopause, distant tail, dawn and dusk tail, and dawn and dusk plasma sheet.

3. Distribution of Particle Destinations

[30] Relevant solar wind, IMF, and SuperDARN ion convection data were available for the five magnetic storms selected for analysis in the present study. These five storms spanned the period of 2000–2005 and the maximum and declining phases of SC 23, as well as the different seasons.

3.1. The 6 April 2000 Event

[31] Figure 2 shows the geomagnetic and solar wind conditions preceding and during the 6 April 2000 storm, including the 3-h K_P index, 1-min symmetric disturbance field in the horizontal component SYM-H, and the time-shifted solar wind data from ACE, including the solar wind dynamic pressure P_{dyn}, IMF B_Y and B_Z. The rapid decrease in SYM-H starting near 1645 UT coincided with the sudden, ten-fold increase in the solar wind dynamic pressure, and the southward turning of the IMF, which resulted in the decrease of B_Z from about −2 nT to −20 nT. The rapid decrease signaled the onset of the main phase at this time. Note that the SYM-H is essentially the same as the Dst index [*Sugiura and Poros*, 1971] and that the time shift in the solar wind data is based on the measured solar wind velocity at ACE and is therefore subject to some uncertainty. In the immediately preceding quiet time period, K_P increased from 3 at 1200 UT to 6 at 1500 UT. The IMF was initially weakly southward ($B_Z \approx$ a few nT negative) and then turned northward around 1430 UT while B_Y was small and dawnward

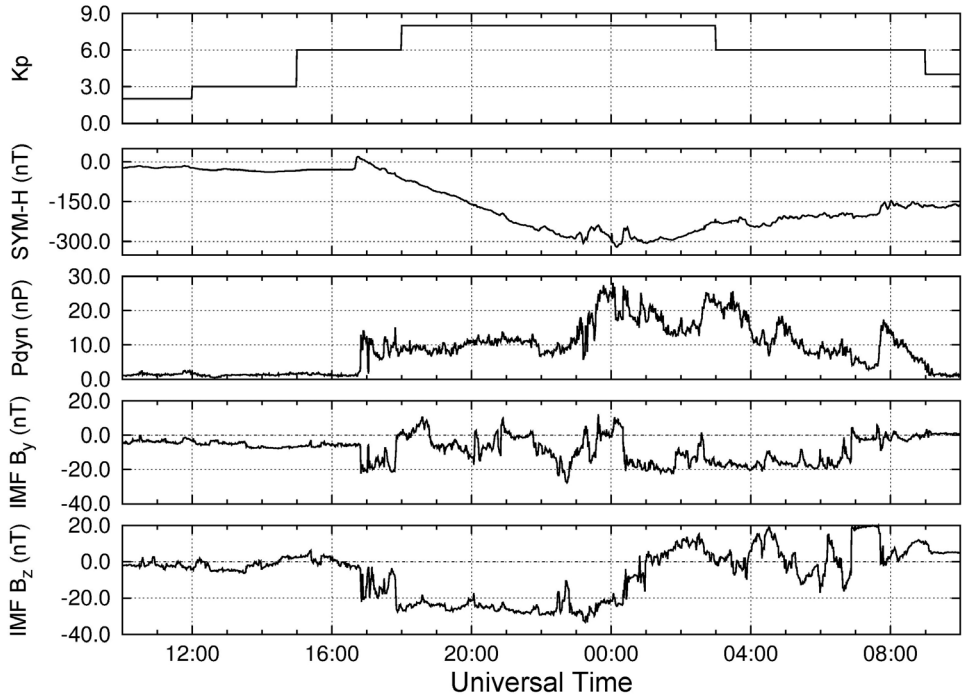

Figure 2. Geomagnetic and solar wind conditions preceding and during the 6 April 2000 magnetic storm (from top to bottom): K_P, SYM-H, solar wind dynamic pressure, and IMF B_Y and B_Z components.

(negative). During the main phase of the storm, K_P reached a maximum value of 8, and SYM-H reached a minimum value of about −320 nT near 0010 UT.

[32] Figures 3a–3c show representative examples of simulated O^+ ion trajectories for this event, using the guiding-center (equations (2) and (3)) and full equations of motion (equation (1)) in the adiabatic and non-adiabatic regions, respectively. Figure 3a shows trajectories for ions starting at 1300 UT and originating at 75° invariant and 12 MLT, with initial energies of (a) 0.5, (b) 1.0, (c) 1.5, (d) 2.0, and (e) 3.0 eV, respectively. In this figure, the color of each trajectory trace denotes the initial ion energy. Each trajectory is projected onto the equatorial (X_{GSM}–Y_{GSM}) and noon-midnight (X_{GSM}–Z_{GSM}) plane. The lowest-energy ions followed trapped trajectories as they did not have sufficient energy to overcome gravitation before reaching the centrifugal acceleration altitude. In contrast, the higher-energy (2 and 3 eV) ions were able to reach the centrifugal acceleration altitude, where they started to gain energy. The highest-energy (3-eV) ion crossed the PSBL and reached the dusk plasma sheet farther down tail compared with the 2-eV ion.

[33] Figure 3b shows the energy evolution of the 2- and 3-eV ions along their respective trajectories in the adiabatic region. In this figure, the instantaneous ion energy in each case is color-coded in logarithmic scale as the ion traversed from the starting location at 7000 km altitude to the PSBL. In the case of the 3-eV ion, the ion energy initially decreased to ∼1.5 eV when the magnitude of centrifugal ion acceleration was insufficient to compensate for the effect of gravitation as the trajectory trace changed in color gradually from green to blue. However, the energy stopped decreasing and instead started to increase as the ion reached higher altitude, to ∼2.5 and >5 eV by the time the ion reached ∼3 and 5 R_E altitude (Z_{GSM} ∼ 4 and 6 R_E), respectively; correspondingly, the trajectory trace gradually reverted back to green starting at 3 R_E and changed to light green at 5 R_E altitude. The ion energy eventually reached 40 eV (and the trace changed to yellow) by the time the ion reached X_{GSM} = −20 R_E. In comparison, the 2-eV ion reached the PSBL at a closer distance (X_{GSM} ∼ −15 R_E), and at a much lower energy (<5 eV). The difference between the two cases may be attributed to the dependence of the magnitude of ion acceleration on the parallel ion velocity in equation (4).

[34] Figure 3c compares the trajectories of 2-eV ions originating from 4 different locations: (a) 80° invariant, 12 MLT; (b) 75° invariant, 12 MLT; (c) 75° invariant, 10 MLT; and (d) 75° invariant, 14 MLT. In this figure, the color of each trace denotes the originating location. Note that the second of these four trajectories is the same as trajectory (d) in Figure 3a. Compared with the ion in this trajectory the other ions traversed regions of smaller magnetic field curvature as they traveled upward along the field line, and consequently experienced lesser centrifugal acceleration. Also, the two ions originating at 10 and 14 MLT (c and d) traversed primarily the dawn and dusk portions of the magnetosphere, respectively, while the ion originating from 75° invariant at 12 MLT (b) followed a predominantly noon-midnight trajectory. In comparison, the ion originating from 80° invariant experienced the least amount of centrifugal acceleration, and its trajectory was confined to a small radial distance at all times.

[35] The guiding-center equation of motion (equations (2) and (3)) was used exclusively in the trajectory calculations in Figures 4–8. Figure 4 shows the distribution of ion destinations as a function of the launch time of the ions before and during the storm, starting at 1250 UT, about 4 h before the storm onset at ∼1645 UT. This figure shows the percentage of non-trapped ions arriving at each of the

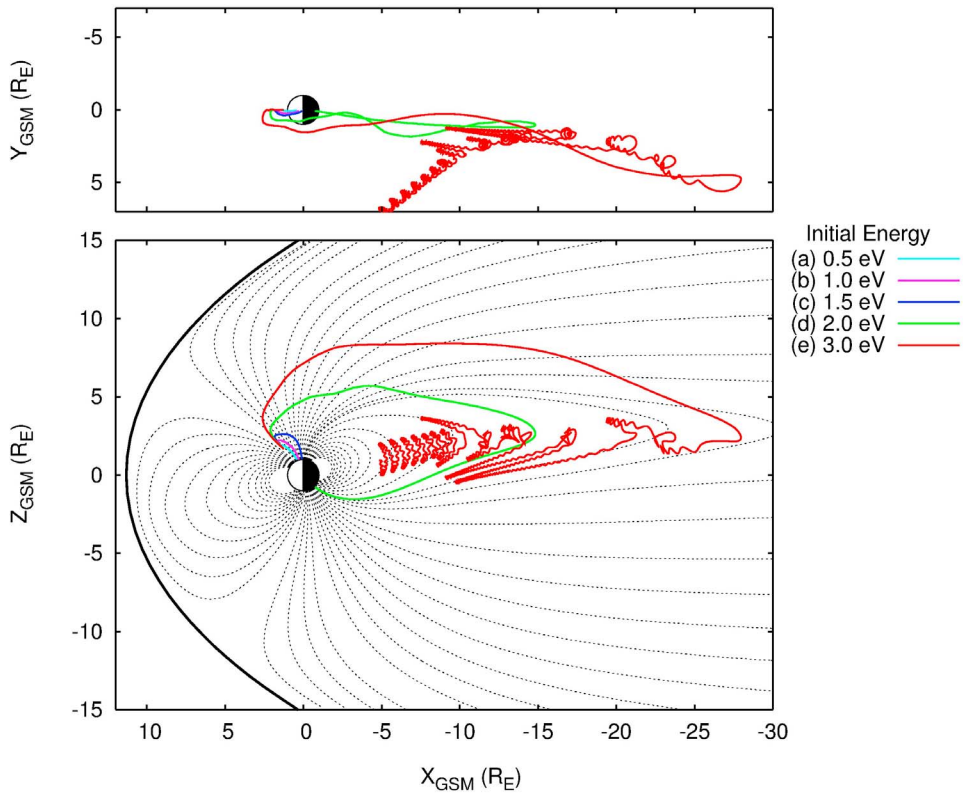

Figure 3a. Examples of simulated trajectories of polar wind O^+ ions originating at 7000 km altitude, 75° invariant and 12 MLT in the storm of 6 April 2000.

7 destinations in the magnetosphere (color traces), and the total percentage of non-trapped ions (black trace). As noted in section 2.2 above, a total of 10,000 ions were launched every 10 min, so that 240,000 ions were launched in all over the 4-h period between 1300 and 1700 UT. Slightly under 35–40% of the ions launched before 1500 UT was un-trapped, when K_P was 3, and the percentage increased slightly to ~40–45% between 1500 and 1800 UT, when K_P increased to 6; see Figure 2 above. About 7–16% of the ions launched before the onset (1645 UT) reached the dusk plasma sheet (blue), while about 3–8% of the ions reached the dawn plasma sheet (purple). The corresponding fractions of ions reaching the dusk and dawn sectors of the tail (gold and red) were comparable and the fractions reaching the dayside and the magnetopause (brown and green) were smaller in comparison. In other words, in the 4-h quiet time period immediately preceding the start of this storm about 10 to 24% of the polar wind O^+ ions originating from 7000 km altitude was found to reach the plasma sheet.

[36] Ions launched at a given time and source altitude generally arrive at their respective destinations at different times, since the travel time of each O^+ ion from its source location to its destination varies with its initial ion position and velocity, and depends on the geomagnetic and solar wind conditions, both of which affect the overall ion convection and ion trajectory. This can be seen in Figure 5, which shows the number of ions arriving at each destination as a function of the arrival time of the ions at the destination, irrespective and instead of the launch time of individual ions. Thus, for example, the distribution at 1500 UT includes ions launched at 1300 UT that had a travel time of 2 h, as well as those launched at 1240 UT that had a travel time of 2 h and 20 min, in other words ions launched 20 min earlier and traveling for 20 min longer. In this figure, each of the 7 color traces denotes the same destination as in Figure 4, but in contrast to Figure 4, the black trace denotes the number of trapped ions in the atmosphere instead of the total number of un-trapped ions in the 7 magnetospheric destinations.

[37] Figure 5 shows a gradual build-up of the number of trapped ions before 1540 UT and a gradual decrease after 2100 UT, which reflect the increasing accumulation of ions launched starting at 1240 UT and the cessation of ion launch at the end of the simulation, respectively. As explained in section 2.2 above, an ion is identified as "trapped" in the *atmosphere* if it was gravitationally trapped or if it descended below 600 km or was below 1 R_E altitude after two hours. Figure 5 also shows a sharper decrease in the percentage of trapped ions and sharper increase in the percentage of un-trapped ions compared with Figure 4 immediately before the storm onset. The sharper decrease in the trapped ion percentage reflects the increasing fraction of ions being accelerated and becoming un-trapped as the strength of convection electric field increased with time in the period immediately before the storm onset.

[38] By the time of the storm onset (1645 UT), more than 10% of the ions were un-trapped and reached the different regions of the magnetosphere. The number of ions reaching the dusk and dawn plasma sheet (blue and purple traces)

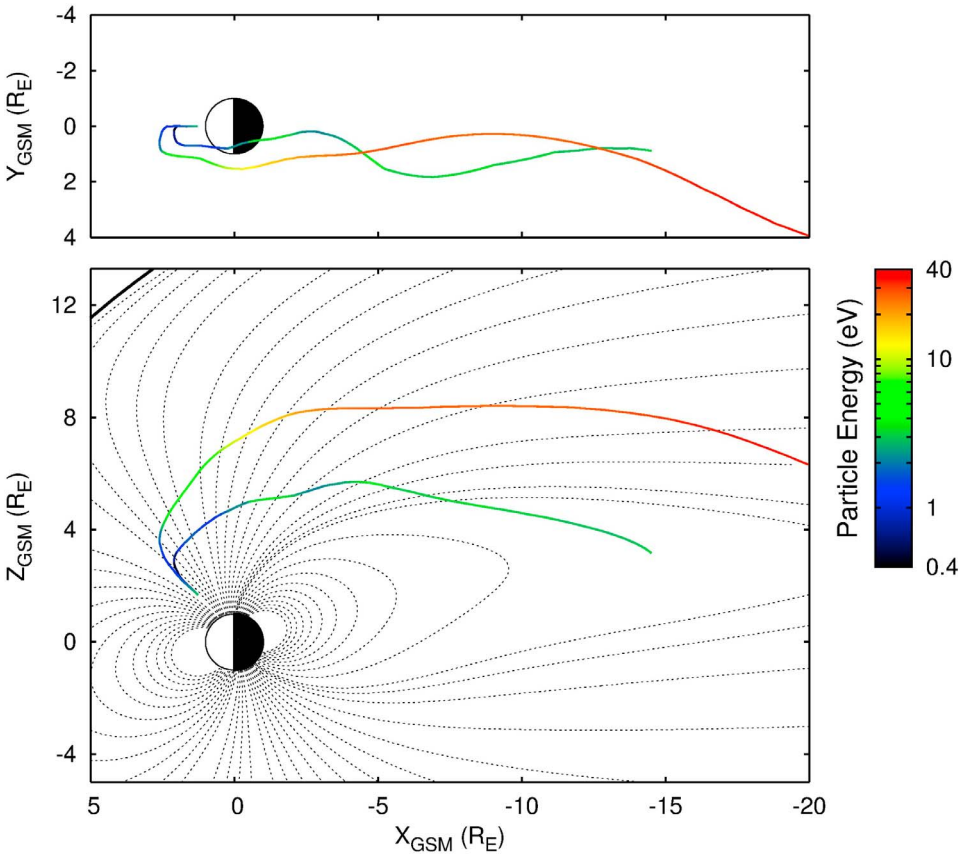

Figure 3b. Energy of polar wind O^+ ions originating at 7000 km altitude, 75° invariant and 12 MLT, and starting at 2- and 3-eV, respectively, along their respective trajectories in the adiabatic region.

peaked around 1900 UT, about 2 h after the storm onset; at this time, the ratio of un-trapped ions reaching the plasma sheet to trapped ions in the atmosphere was about 0.45. This implies that about 20% of the polar wind O^+ ions launched a few hours earlier had reached the plasma sheet by this time.

[39] The green trace in Figure 5 denotes the number of ions that "hit the magnetopause," including (as explained in section 2) ions that reached the magnetopause or its vicinity, where the field lines did not connect back to the ionosphere in the Tsyganenko 1996 (T96) model. This trace exhibits a sharp spike at the time of arrival of the solar wind pressure pulse at 1645 UT; cf. Figure 2. A detailed analysis of the simulation results shows the sudden compression of the magnetosphere at this time, when the magnetopause was pushed inward (earthward) by more than 1 R_E within the 10-min time interval between successive electric and magnetic field updates in the simulation. This resulted in the ions that were in the vicinity (within 1 R_E) of the magnetopause in the different magnetospheric regions suddenly finding themselves arriving at or inside the magnetopause as the magnetosphere compressed suddenly—and hence a sudden increase in the number of ions that are designated as "hitting the magnetopause."

[40] To examine the detailed characteristics of the simulated O^+ ions that reached the plasma sheet and the magnetotail, Figure 6 shows the spatial and energy distributions of these ions as a function of X_{GSM} and Y_{GSM}. Each dot (data point) in this figure denotes an ion that was launched during the 8-h simulation period (1250–2050 UT) and subsequently reached the plasma sheet or magnetotail; the position of each dot denotes the X_{GSM} and Y_{GSM} coordinates of the ion while its color represents the ion energy.

[41] A total of about 148,000 ions (about 31% of the 480,000 ions launched) are shown in Figure 6, and the density of the data points in the figure depicts qualitatively the spatial distribution of the simulated O^+ ions, which is expected to approximate the corresponding ion density distribution, given the nature of the Monte Carlo selection of initial particle phase space. Thus, it can be seen that the ion density in the plasma sheet was higher than that in the magnetotail, and that in both regions, the density was higher in the dusk sector.

[42] Likewise, the dominant color in the respective areas of Figure 6 depicts the averaged ion energy in the different regions of the plasma sheet and magnetotail. Thus, it can be seen that the averaged ion energy of the O^+ ions increased with decreasing $|X_{GSM}|$, and that the ions reached keV energy as they crossed the PSBL. In addition, the ions along or near the midnight meridian ($|Y_{GSM}| < 5$ R_E) tended to have higher energies than those further away from the meridian ($|Y_{GSM}| > 5$ R_E). This trend is consistent with the

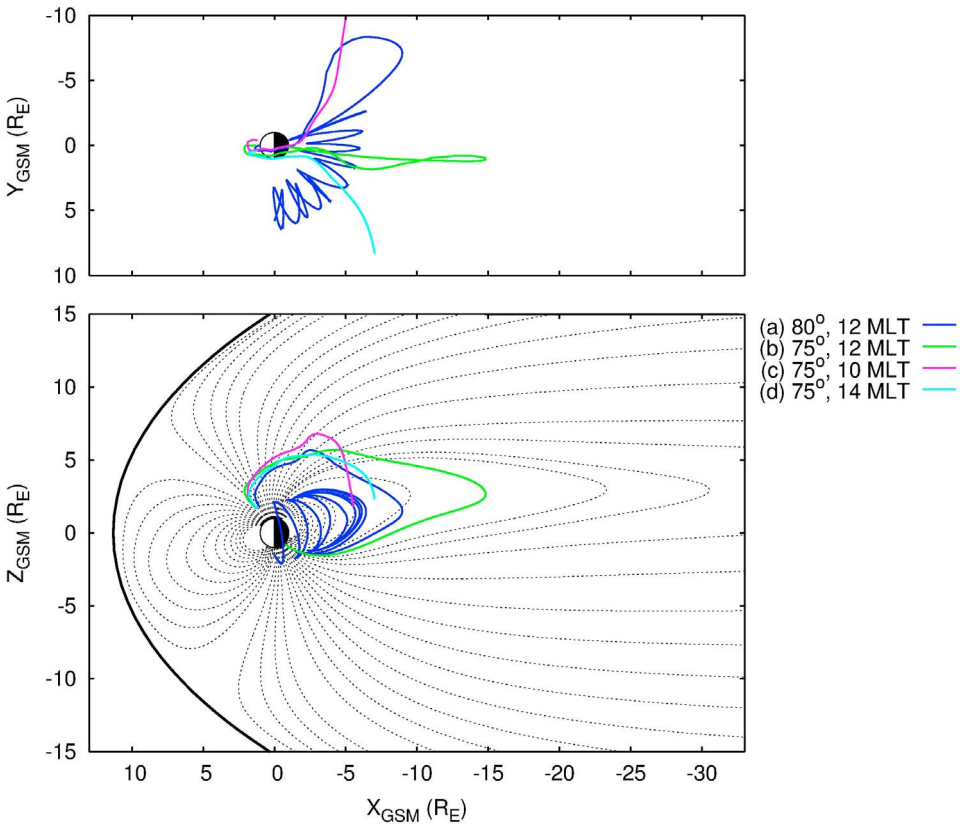

Figure 3c. Simulated trajectories of 2-eV polar wind O^+ ions originating from different invariant latitude and MLT locations at 7000 km altitude.

pattern of less ion acceleration away from the magnetic local noon in Figure 3c above.

3.2. Comparison of Storms

[43] Figures 4–6 show that in general a variable but non-negligible fraction of thermal-energy O^+ ions can become un-trapped and reach the magnetosphere in the period immediately before the onset of the main phase of a magnetic storm. The distribution of such un-trapped ions in the different regions of the magnetosphere is expected to be dependent on the prevailing geomagnetic and solar wind conditions. To examine this dependence in the five storms in the present study, Figure 7 shows the 3-h K_P index, 1-min SYM-H, and time-shifted ACE data of solar wind dynamic pressure, P_{dyn}, IMF B_Y and B_Z preceding and during the five storms: these storms occurred on 6 April 2000 (storm A), 6 November 2000 (storm B), 5 November 2001 (storm C), 29 May 2003 (storm D), and January 21 2005 (storm D), respectively. To facilitate data comparison, the data for the five storms are shown in different colors in each data panel, and offset with respect to the onset time of the main phase of each storm, i.e., the time when Dst started to turn negative or to decrease sharply in the case of a storm with and without a SSC, respectively.

[44] Table 1 summarizes the time of storm onset, the minimum Dst (SYM-H) value, and the time of rapid increase and the maximum value of solar wind dynamic pressure (P_{dyn}) in each of the 5 storms studied (columns 3 to 6), as well as the range of IMF B_Y and B_Z in the 4-h period following and preceding the onset, respectively (columns 7 to 10), for comparison with the distribution of ion destinations in the magnetosphere in each storm, including the percentage of ions that reached the dusk and dawn plasma sheet and tail, respectively (columns 11 to 14).

[45] The first three of the five storms (storms A to C) were near the maximum phase of SC 23, while the remaining two (storms D and E) occurred in the declining phase of the cycle; as noted earlier, non-recurrent magnetic storms occur most frequently at solar maximum, while recurrent storms occur most frequently in the declining phase of a solar cycle. Together, the five storms spanned the four seasons of the year, occurring in spring, late fall, late fall, early summer, and late winter, respectively.

[46] Based on the criterion of the minimum Dst value of a "moderate," "large," and "super" storm being less than −50, −100, and −250 nT, respectively, the five storms include a "moderate" storm with a minimum Dst of ∼ −100 nT (storm E) and two "super-storms" with a minimum Dst below −320 nT (storms A and C), the other two storms (storms B and D) being "large" storms with a minimum Dst of ∼−170 nT. The first three storms (storms A to C) are identified as isolated storms in that Dst was above −50 nT for several hours immediately preceding the storm in each case. Storm E is also treated as an isolated storm for the

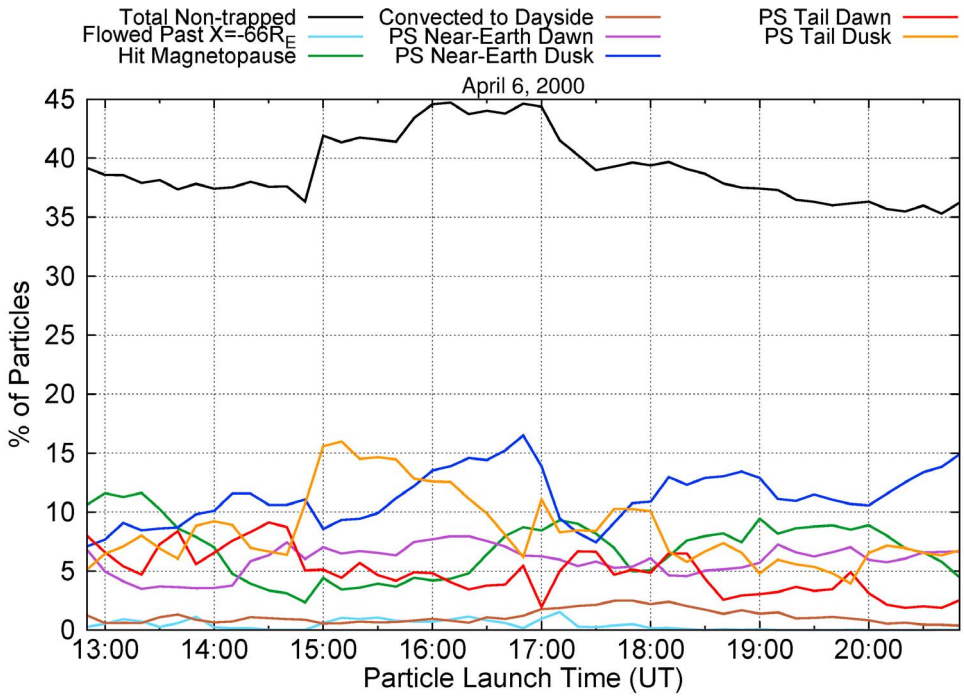

Figure 4. Distribution of simulated ion destinations in terms of the percentage of ions at each destination (region of the magnetosphere) as a function of the launch time of the ions before and during the 6 April 2000 magnetic storm: the dayside (brown), magnetopause (green), distant tail ($X < -66\ R_E$; light blue), dawn and dusk tail (red and gold), dawn and dusk plasma sheet (purple and blue), and total non-trapped (black).

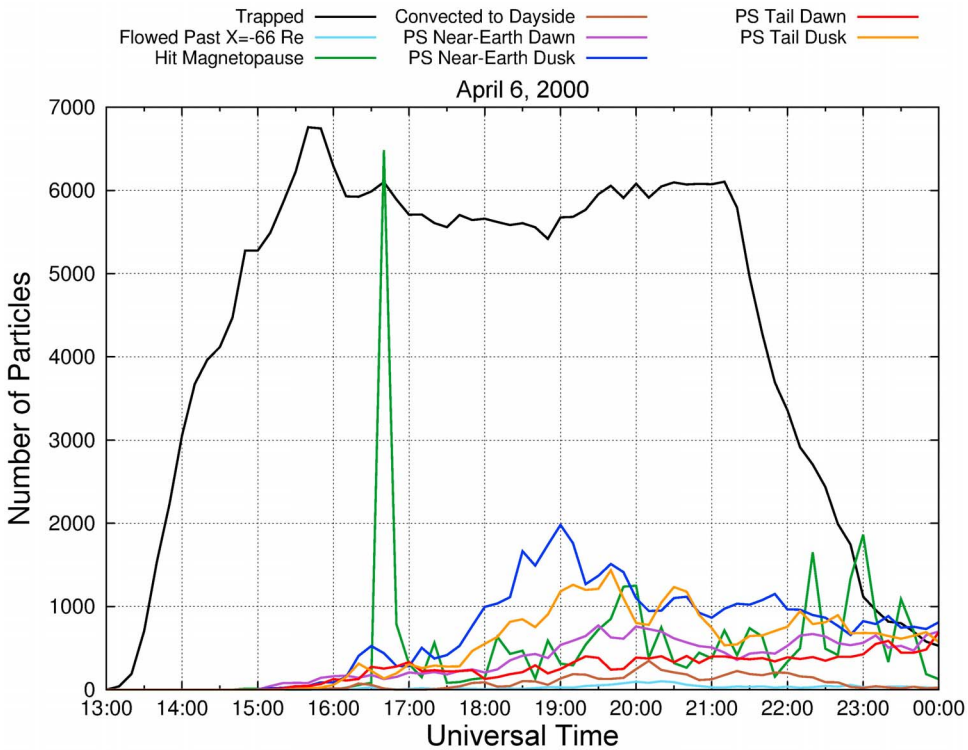

Figure 5. Number of ions arriving at each magnetospheric destination as a function of their arrival time before and during the 6 April 2000 magnetic storm, using the same color codes for the different regions of the magnetosphere as in Figure 4; the black trace denotes the number of trapped ions in the atmosphere.

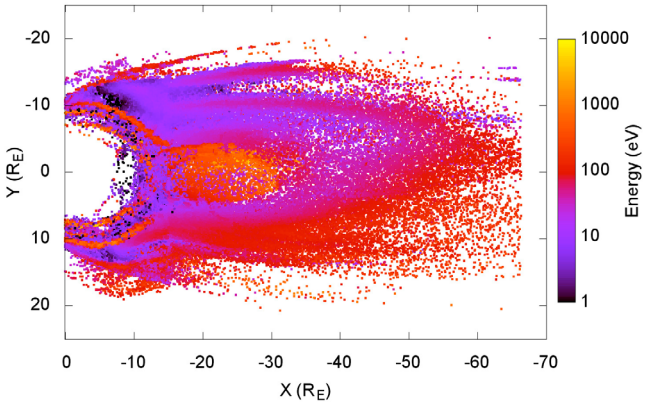

Figure 6. Distribution of about 148,000 simulated O^+ ions that reached the plasma sheet or the magnetotail in the magnetic storm of 6 April 2000.

purpose of this study despite the very brief excursion of SYM-H to a value near −50 nT within an hour of the onset. In contrast, storm D appears to consist of a sequence of three overlapping storms with the second and third onset 4:40 and 5:30 after the first onset, respectively, and the three storms had minimum Dst values of −80, −100, and −170 nT, respectively.

[47] In the context of thermal-energy plasma transport in the period immediately preceding the main phase of a storm, a number of differences in the geomagnetic and solar wind conditions are noteworthy between the five storms, including those in Figure 7 and Table 1. First, the initial phase (SSC) was present before the onset of the main phase of the storm in the case of storms A, C, and E, and possibly also D; in all four cases, Dst increased to 10–20 nT, and the value of AE was <1000 nT (not shown). In contrast, in the case of storm B, Dst remained negative and below −30 nT for several hours immediately before the storm onset; in this

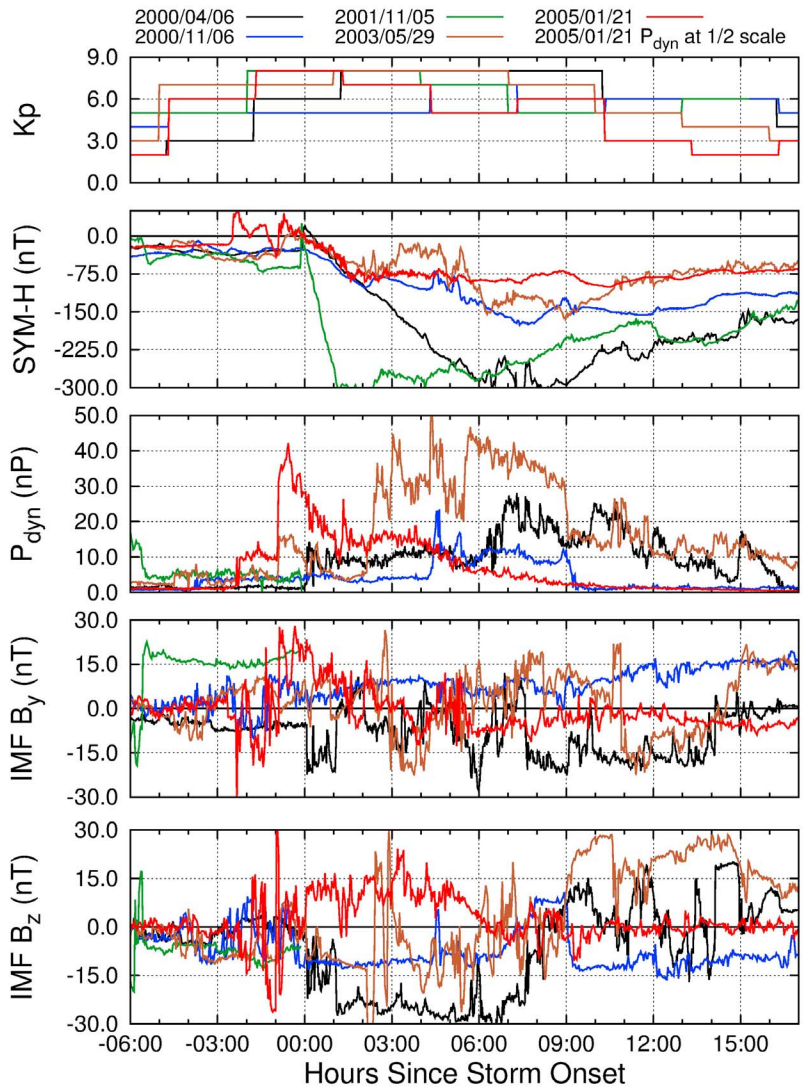

Figure 7. (top to bottom) The 3-h K_P index; 1-min SYM-H; and time-shifted ACE data of solar wind dynamic pressure, P_{dyn}, IMF B_Y and B_Z, preceding and during five magnetic storms on 6 April 2000 (storm A, black), 6 November 2000 (storm B, blue), 5 November 2001 (storm C, green), 29 May 2003 (storm D, brown), and 21 January 2005 (storm E, red; with P_{dyn} displayed in half scale), respectively.

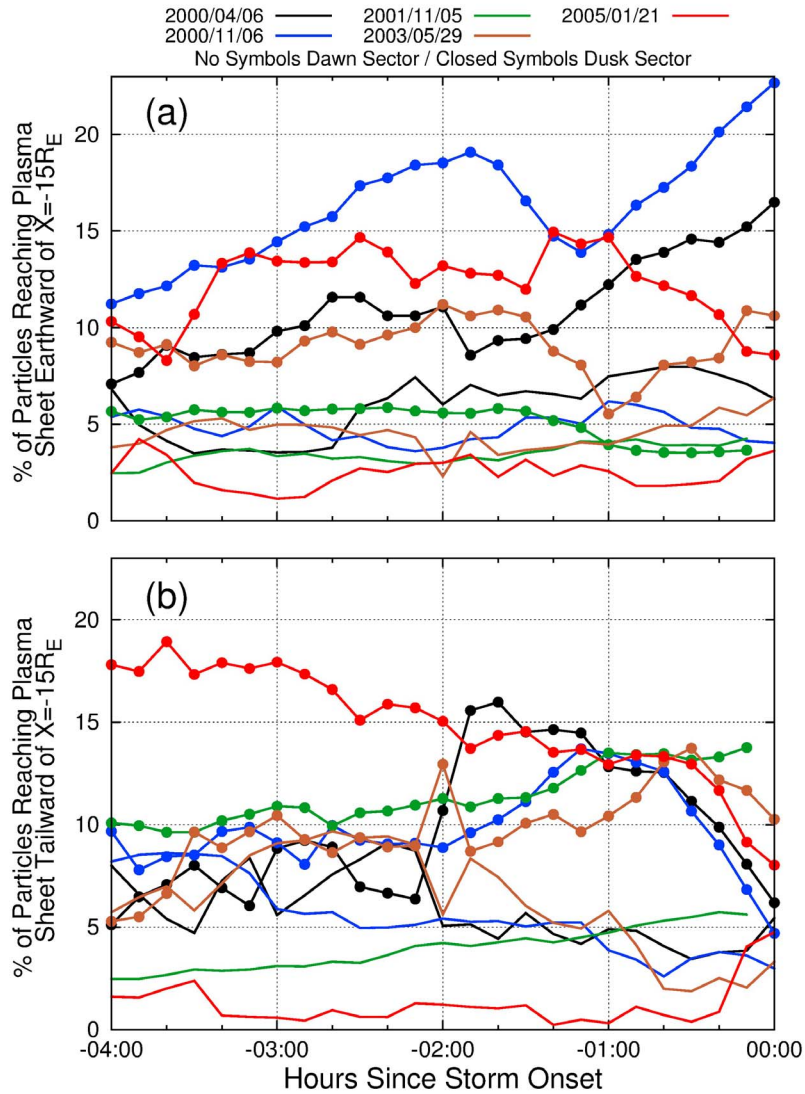

Figure 8. Percentage of un-trapped thermal-energy O^+ ions reaching the dusk (solid circles) and dawn (no circles) sectors of the (a) plasma sheet and (b) magnetotail, as a function of the launch time of the ions relative to the onset of the main phase of the magnetic storms on 6 April 2000 (storm A, black), 6 November 2000 (storm B, blue), 5 November 2001 (storm C, green, with the data display shifted to the right by 2 h in the figure to show data 2–6 h before the onset), 29 May 2003 (storm D, brown), and 21 January 2005 (storm E, red), respectively.

case, the AE index was much larger and exceeded 3000 nT in the 4-h period before the onset, and was indicative of strong substorm activities.

[48] Second, the onset of the main phase did not always coincide with the sudden enhancement in solar wind dynamic pressure and the southward turning of the IMF. Table 1 shows that the onset approximately coincided with the sudden rise in P_{dyn} in the case of storm A, but the two events were almost an hour apart in storm E. Data of P_{dyn} was not available at the time of onset in storm C. In the case of storm D, in which successive onsets occurred at 1700, 2140, and 2230 UT, three successive rises in P_{dyn} were observed at 1610, 2120, and 2240 UT. In other words, the last two onsets were within 15 min of the corresponding rise in P_{dyn} while the first onset and P_{dyn} rise were about 50 min apart.

[49] Third, the minimum Dst ranged from ~ -100 to -320 nT while the maximum solar wind dynamic pressure during the main phase ranged from $\sim$5 to 85 nP; note that in Figure 7, P_{dyn} is displayed in half scale (as $0.5 \times P_{dyn}$) in the case of storm E in order to make the data for the other storms more legible.

[50] Fourth, both the B_Y and B_Z components of the IMF were quite variable in some of the storms in the 4-h periods immediately preceding and following the onset, which, as noted above, did not coincide with the southward turning of the IMF in every storm. IMF was predominantly southward (B_Z was negative) most but not all of the time both before and after the onset in storm A. In contrast, it was highly variable in polarity but on balance northward (B_Z was positive) before the onset in storm B and E; in the case of storm E, the level of activity was moderate (Dst ~ -100 nT) despite

Table 1. Solar Wind Pressure, IMF, and Simulated Thermal O^+ Ion Percentage in Magnetic Storms

Event ID and Date	Onset Time (UT)	Min Dst (nT)	Time of Rapid P_{dyn} Increase (UT)	Max P_{dyn} (nP)	After Onset		Before Onset		Averaged Percentage (Range) of Un-trapped Ions Launched Before Onset				
									Plasma Sheet		Tail		
					B_Z (nT)	B_Y (nT)	B_Z (nT)	B_Y (nT)	Dusk	Dawn	Dusk	Dawn	Total
A 2000/04/06	1645	−320	1645	12	−30 to −10	−20 to 10	−5 to 5	−2 to −8	10.9 (7–16)	5.9 (3–8)	9.8 (4–16)	5.8 (2–9)	32.4 (24–38)
B 2000/11/06	1340	−175	1430	5	−12 to 9	0 to 10	−10 to 10	−10 to 10	16.2 (11–23)	4.8 (4–6)	9.8 (5–14)	5.5 (3–9)	36.4 (34–39)
C 2001/11/06	0200	−300	N/A	N/A	N/A	N/A	−12 to −5	15 to 20	5.1 (4–6)	3.5 (2–4)	11.4 (10–14)	3.9 (2–6)	23.9 (20–27)
D 2003/05/29	1700	−80	1610	17	−32 to 30	−22 to 28	−10 to 10	−10 to 10	9.0 (6–11)	4.5 (2–6)	9.8 (5–14)	6.2 (2–10)	29.6 (24–33)
	2140	−100	≤2125	≤50	−26 to 20	−12 to 20							
	2230	−170	2240	46	−16 to 17								
E 2005/01/21	1940	−100	1850	85	−2 to 22	−12 to 22	−25 to 30	−30 to 28	12.2 (8–15)	2.5 (1–4)	14.9 (8–19)	1.2 (0–5)	30.8 (25–33)

the large solar wind dynamic pressure (P_{dyn} = 85 nP); this may perhaps be attributed to the mostly northward IMF at the time of solar wind pressure enhancement. In storm D, it was mostly northward before the first onset at 1700 UT, but underwent several changes in direction afterwards.

[51] Fifth, the B_Y component of the IMF was predominantly dawnward (negative) and duskward (positive) in storm A and C, respectively, before the onset, and it remained predominantly dawnward for the first hour after the onset in storm A, when its magnitude increased from less than 5 nT to ∼20 nT; solar wind particle data was not available for the determination of P_{dyn} and the time-shifting of the IMF data after the onset in storm C. In contrast, B_Y was variable before the onset in storms B, D, and E, and remained variable after the onset in storm D and E but became predominantly duskward (positive) in storm B.

[52] Figure 8 compares the distribution of thermal-energy O^+ ions in the (a) plasma sheet and (b) magnetotail in the five storms. As in Figure 7, the data for the different storms are shown in different colors and with respect to the onset time of the main phase of each storm. In each panel, the percentage of ions reaching the dusk and dawn sector is shown separately, with and without the solid circles, respectively, and as a function of the launch time of the ions, 0–4 h before the storm onset except in the case of storm C.

[53] In the simulation, ions that were gravitationally trapped or otherwise remained below 1 R_E altitude after 2 h were identified as "trapped," and most of the "un-trapped" ions reached their magnetospheric destinations within 4 h after their launch. Therefore, in general, IMF and solar wind parameter data were required for the 4-h period after the time of an ion launch, to update the electric and magnetic field distributions for the purpose of computing the ion trajectory. In the case of storm C, where the required solar wind plasma pressure data for the simulation was available only before the onset, the IMF and solar wind parameters were assumed to remain unchanged in the first 2 h after the onset, and the data is displayed for ions launched 2–6 h before the onset and shifted to the right by 2 h in the figure. In other words, the computed distributions for ions launched between 4 and 2 h before the onset of storm C are shown on the right half of the green traces (between −02:00 and 00:00) in Figure 8, and they are believed to be approximate and may be in error due to variations in IMF and P_{dyn} in the first two hours after the onset.

[54] Figure 8 shows that in all five storms, a variable percentage of the thermal-energy O^+ ions that were launched in the quiet time period immediately preceding the storm onset reached both the dawn and dusk sectors of both the plasma sheet and the magnetotail. The percentage varied from ∼20% to 39% and averaged to about 24–36% within each of the five storms studied. The percentage in the plasma sheet was ∼30–40% larger than that in the magnetotail in storms A and B, and about 10–45% smaller in the other three storms (C, D and E). In other words, about 17–21% of the ions reached the plasma sheet in storms A and B compared with 9–15% in storms C, D and E.

[55] A dawn-dusk asymmetry in favor of the dusk sector is apparent in four of the five storms: the dusk-to-dawn percentage ratio averaged 2.7 and ranged from 1.5 in storms A, B and D to 4.9 in storm E in the plasma sheet, and averaged 4.1 and ranged from 1.6 to 12.4 in the magnetotail.

[56] The differences between the storms in their respective percentages of ions reaching different regions of the magnetosphere may be attributed to a number of factors. First, the overall percentage of un-trapped ions is expected to depend crucially on the magnitude of centrifugal ion acceleration below the "turnaround" altitude, where an $\mathbf{E} \times \mathbf{B}$ convecting ion with less than escape velocity will lose all of its initial kinetic energy to gravitation and fall back to the atmosphere in the absence of any acceleration. It can be seen in equations (2) and (4) that for an $\mathbf{E} \times \mathbf{B}$ convecting ion, the amplitude of ion acceleration due to a changing magnetic field increases with increasing $\mathbf{E} \times \mathbf{B}$ velocity and/or increasing changes to the magnetic field in the $\mathbf{E} \times \mathbf{B}$ direction. This implies that an increase in the amplitude of IMF B_Y and/or B_Z would result in an increase in the overall amplitude of convection electric field, particularly under southward IMF conditions [*Shepherd and Ruohoniemi*, 2000], and lead to larger centrifugal acceleration of the thermal-energy ions below the turnaround altitude and ultimately a larger percentage of ions being able to reach the different regions of the magnetosphere. Likewise, for a given $\mathbf{E} \times \mathbf{B}$ convection strength, the percentage of un-trapped ions is expected to increase with an increasing rate of change of the magnetic field. Note, however, that a larger overall un-trapped percentage does not necessarily lead to a larger ion percentage in the plasma sheet and magnetotail in Table 1, which does not include the percentage of ions reaching the dayside or the magnetotail beyond $X_{GSM} < -66$ R_E.

[57] Second, for a given overall percentage of un-trapped ions reaching the magnetosphere, the relative proportion between those reaching the plasma sheet and the magnetotail is expected to depend on the amplitude and polarity of the IMF, which control both the strength and the configuration of $\mathbf{E} \times \mathbf{B}$ convection. In particular, the increased strength of $\mathbf{E} \times \mathbf{B}$ convection under strongly southward IMF is expected to result in proportionally more of the un-trapped ions from the dayside reaching further down tail, and more of those from the night side reaching lower L-shells. This in turn leads to a larger percentage of un-trapped ions reaching the magnetotail compared with the plasma sheet, since the fraction of un-trapped ions is larger on the dayside on average. This can be seen to be the case in Table 1 between storm C, in which B_Z was strongly southward for an extended duration before the onset and the plasma sheet to magnetotail ratio of un-trapped ions was about 0.56, and storm A, in which B_Z was northward or weakly southward and the corresponding ratio was 1.1.

[58] Third, the solar wind dynamic pressure may also be an important factor in the plasma sheet to magnetotail ratio of the un-trapped ion percentage, depending on the prevailing IMF conditions (strength and polarity) and the resulting degree of coupling between the IMF and the Earth's internal field. This is because as P_{dyn} increases under southward IMF conditions, the magnetosphere becomes increasingly compressed and the magnitude of the convection electric field also increases [*Shepherd and Ruohoniemi*, 2000], resulting in larger centrifugal ion acceleration and stronger $\mathbf{E} \times \mathbf{B}$ convection, and ultimately a larger overall percentage of un-trapped ions reaching the magnetosphere and a larger magnetotail to plasma sheet percentage ratio; P_{dyn} is expected to be less of a factor under northward IMF conditions. Likewise, the rate at which P_{dyn} increases can also play a significant role, since a more rapid rise in P_{dyn} results in a more rapid change in the magnetic field, which in turn leads to a larger increase in the overall percentage of un-trapped ions, as discussed above.

[59] Fourth, the polarity of IMF B_Y is expected to affect the relative ratio of un-trapped ion percentage between the dawn and dusk magnetosphere, and the latter is expected to dominate on average. As shown previously in *Howarth and Yau* [2008], the ions preferentially feed the dusk sector of the plasma sheet when the IMF is duskward ($B_Y > 0$), and are more evenly distributed between the dusk and dawn sectors when the IMF is dawnward ($B_Y < 0$). Indeed, in Table 1, the dusk-to-dawn ratio of the percentage in the plasma sheet ranges from 1.5 to 4.9 and averages 2.7, while the ratio in the magnetotail ranges from 1.6 to 12.4 and averages 4.1. The ratio for the plasma sheet and magnetotail combined averages to 3.1, and varies from 1.7 in storm A, in which B_Y was predominantly dawnward (negative), to 7.3 in storm E, in which B_Y was predominantly and strongly duskward and as large as 28 nT in the 2 h immediately preceding the onset. In other words, the dusk-to-dawn ratio of the un-trapped ion percentage is generally higher when the IMF is duskward.

[60] Finally, the average parallel velocity of the polar wind O^+ ions, which varies with the overall level of geomagnetic activity as characterized by the K_P index, is expected to affect both the overall percentage of trapped ions and the plasma sheet to magnetotail percentage ratio. As shown in Figure 1, the observed parallel ion velocity at the starting altitude is dependent on K_P; in our simulation model, it is typically a factor of 1.5–2.0 higher under high-K_P conditions. This results in a larger percentage of ions gaining sufficient energy to overcome gravitation before reaching the turnaround altitude for a given level of centrifugal acceleration. At the same time, the larger initial parallel velocity also results in proportionally more of the un-trapped ions remaining at higher L-shells as they reach the magnetosphere for a given ion convection strength, and ultimately leads to a smaller plasma sheet to magnetotail percentage ratio. It is clear that these five factors combine to affect the overall distribution of un-trapped thermal-energy O^+ ions in the quiet time period immediately preceding a magnetic storm. However, because of the relatively small number of storms studied, it is beyond the scope of this study to quantitatively delineate the relative importance of these five factors.

4. Discussion and Summary

[61] In sections 2 and 3 above, we extended the simulation model in *Howarth and Yau* [2008] to the case of time-dependent magnetic and convection electric field, to study the transport of thermal-energy polar wind O^+ ions in the quiet time periods immediately preceding the main phase of five magnetic storms, when the IMF sometimes varies rapidly in polarity. Our study includes 2 large storms (minimum Dst < -100 nT) and 2 "super-storms" (minimum Dst < -300 nT), and storms in both the maximum and the declining phase of SC 23.

[62] The simulation used the guiding-center equations of motion (equations (2) and (3)) to solve for the single-particle trajectories of a number of ions starting from the high-

altitude polar ionosphere during the 4-h period preceding the onset of each storm, to determine the fraction (percentage) of ions that was able to overcome gravitation and reach the different regions of the magnetosphere as a result of centrifugal ion acceleration at higher altitudes. Every 10 min in the 4-h period, the IGRF internal and Tsyganenko 1996 external magnetic field and the SuperDARN convection electric field models were updated, with a linear interpolation in between, and a total of 10,000 ions were "launched" from the starting altitude of 7000 km; a Monte Carlo technique was used to randomly select the initial position (invariant latitude and MLT) and velocity for each ion to ensure a statistically representative sampling of the ion phase space consistent with the observed polar wind ion velocity and temperature on Akebono [*Drakou et al.*, 1997; *Abe et al.*, 2004].

[63] The result of our simulation is summarized as follows:

[64] 1. In the case of polar wind oxygen ions under typical quiet time geomagnetic and solar wind conditions, the lowest-energy ions (≤2 eV) did not have sufficient energy to overcome gravitation before reaching the centrifugal acceleration altitude, but the higher-energy (>∼2 eV) ions were able to do so and subsequently experience further acceleration and reach the magnetosphere at ∼10 R_E or beyond (Figure 3a): Ions originating at or near 75° invariant and 12 MLT experienced larger acceleration as they traversed regions of larger magnetic field curvature compared with those originating at higher invariant latitudes or other magnetic local times (Figure 3c).

[65] 2. A variable and small fraction (up to ∼24–36%) of the ions launched in the 4-h period preceding a storm onset could overcome gravitation and become un-trapped and reach the plasma sheet and magnetotail (Figures 4 and 8 and Table 1); roughly a quarter of these ions is estimated to have reached the plasma sheet or magnetotail by the time of the storm onset (Figure 5), since their most probable and medium travel time were found to be about 3.4 and 4.3 h, respectively.

[66] 3. On average, the dusk sector dominated the percentage of un-trapped ions in the plasma sheet and magnetotail. The ratio of un-trapped ions between the dawn and dusk magnetosphere was affected by the polarity of IMF B_Y, the dusk-to-dawn ratio of the percentage being in the range of 1.7 to 7.3 and 3.1 on average (Table 1 and Figure 8).

[67] 4. The averaged energy of the un-trapped O^+ ions increased with decreasing radial distance ($|X_{GSM}|$) in the magnetosphere, and the ions reached keV energy as they crossed the PSBL (Figure 6).

[68] 5. The distribution (percentage) of un-trapped ions that reached the plasma sheet and the magnetotail was strongly influenced by a number of factors. These included the IMF B_Y and B_Z components, the rate of change of the magnetic field, the solar wind dynamic pressure, and the level of geomagnetic activity as characterized by the K_P index (Table 1 and Figure 8).

[69] 6. An increase in IMF B_Y and B_Z resulted in an increase in the overall strength of $\mathbf{E} \times \mathbf{B}$ convection, particularly under southward IMF conditions, and led to larger centrifugal ion acceleration and ultimately a larger percentage of un-trapped ions.

[70] 7. An increased rate of change of the magnetic field also resulted in larger centrifugal acceleration, and for a given $\mathbf{E} \times \mathbf{B}$ convection strength led to a larger percentage of un-trapped ions.

[71] 8. For a given $\mathbf{E} \times \mathbf{B}$ convection strength an increase in convection strength and/or rate of magnetic field changes also resulted in an increase in the magnetotail to plasma sheet percentage ratio, due to more ions from the dayside becoming un-trapped compared with those from the night side on average, and to more ions from the dayside and night side reaching higher and lower L-shells, respectively.

[72] 9. The effect of the solar wind dynamic pressure on the un-trapped ion percentage was dependent on the prevailing IMF strength and polarity, and was more pronounced under strongly southward IMF conditions.

[73] 10. Under high K_P conditions, the larger initial parallel ion velocity resulted in proportionally more of the un-trapped ions remaining at higher L-shells and ultimately a smaller plasma sheet to magnetotail percentage ratio.

[74] As discussed in *Peterson et al.* [2009], the O^+ ion density in the plasma sheet is highly variable and dependent on magnetic activity level. Near solar minimum on ISEE-1 [*Lennartsson and Shelley*, 1986], the density of O^+ ions above 100 eV was found to range from ∼0.01 at quiet times (AE < 200 nT) to ∼0.1 cm^{-3} at active times (AE ≥ 200 nT) between 10 and 22 R_E, and to peak near $Y_{GSM} = 0$, particularly during active times. In addition, the density was found to exhibit a dawn-dusk asymmetry in favor the dusk sector, the quiet time dusk-to-dawn density ratio being about 2 in the $|Y_{GSM}| < 15\ R_E$ region. Near solar maximum on Cluster [*Kistler et al.*, 2006], the measured O^+ density was ∼0.02 cm^{-3} at 19 R_E in quiet intervals before substorms. The large asymmetry (factor of 1.5 to ∼5 dusk-to-dawn ratio) in O^+ plasma sheet ion density in Figure 8 and Table 1 is clearly in good qualitative accord with the ISEE-1 data at least insofar as dawn-dusk asymmetry, assuming that the observed asymmetry in the ISEE-1 data near solar minimum was not strongly dependent on solar activity level.

[75] On the question of low-energy plasma sheet O^+ ions, the low-energy cut-off of the ISEE-1 ion mass spectrometer (100 eV/e) precluded its detection of O^+ ions below 100 eV, whose presence in the plasma sheet is possible, for example at times of low $\mathbf{E} \times \mathbf{B}$ velocities. On Geotail, cold ions of unknown mass species below 100 eV were frequently observed at comparable densities to the hot ions in the eclipsed regions of the central plasma sheet [*Seki et al.*, 2003]. On Cluster, where the ion composition and distribution function (CODIF) instrument had a 40-eV low-energy cut-off, most of the measured O^+ ions were above 100 eV [*Kistler et al.*, 2005]. Figure 6 suggests that in the absence of other additional acceleration processes, a large fraction of the un-trapped O^+ ions reaching the plasma sheet typically had energies of 100 eV or greater (color-coded in red or orange in Figure 6) due to centrifugal ion acceleration; this appears to be consistent with the Cluster results.

[76] Using Cluster magnetic field and CODIF ion composition data, *Nilsson et al.* [2008] investigated the role of centrifugal ion acceleration in the altitude range of 5–12 R_E, by comparing the accumulated effect of the acceleration over this altitude range with the observed parallel O^+ ion velocity in each of several orbits. It was found that a large fraction of the observed ion velocity may be attributed to

the acceleration, and that the observed velocity was consistent with initial ion energy of about 40 eV (velocity of about 20 km/s) at 5 R_E under realistic ion convection conditions in a steady state magnetic field. Due to spacecraft charging and other technical reasons, the analysis in *Nilsson et al.* [2008] was confined to ion data above 40 eV and focused on acceleration events of higher-energy ions on auroral field lines; it excluded lower-energy ions such as the polar wind whose energy-per-charge was below the spacecraft potential, which was typically in the range of 5–40 V in the polar cap [*Eriksson et al.*, 2006]. In comparison, the two polar wind O^+ ions in Figure 3b above had lower energies (<5 and <10 eV, respectively) by the time they reached 5 R_E. The larger "initial" ion energy on Cluster may be attributed to the dominance of higher-energy ions such as the cleft ion fountain and upwelling ions in the Cluster analysis, which have higher energies than polar wind ions but are not always observationally separable from the polar wind ions, as noted in section 1.

[77] In equations (2) and (4) above, each of the three acceleration terms can in principle give rise to ion acceleration or deceleration in a given instance depending on the relative orientation between the magnetic and convection electric fields and their spatial or temporal gradients. Statistically, ion acceleration due to the parallel and perpendicular terms was observed to be much more frequent compared with ion deceleration on Cluster: the acceleration-to-deceleration occurrence frequency ratio being 2–10 [*Nilsson et al.*, 2008]; the dominance of acceleration over deceleration is not surprising given the topology of the magnetic field at high altitudes. In contrast, the occurrence frequency ratio of ion acceleration due to the temporal term was near unity. On average, the magnitude of ion acceleration due to the parallel and perpendicular terms was about 5 and 3 m s^{-2}, respectively, and larger compared with the temporal term (<2 m s^{-2}) [*Nilsson et al.*, 2008]. This implies that in the case of a time-dependent magnetic field, the parallel and perpendicular terms are expected to dominate the overall effect of centrifugal acceleration, and it explains the modest range of un-trapped ion percentage (24–36%) in Table 1 for the 5 storms, which span a wide range of minimum Dst values and correspond to different time-dependent magnetic and convection electric field conditions. Indeed, the modest range of ion percentages suggests that at times of Dst below −100 nT in a large magnetic storm the possibly reduced accuracy of the T96 model is unlikely to significantly affect the ion percentages or fundamentally alter the overall results of the present study, which is focused anyhow on the pre-storm quiet time period when Dst is within the recommended interval of the model.

[78] The estimated volume of the quiet time plasma sheet is about 4×10^{24} m^3 [*Chappell et al.*, 1987]. The ISEE-1 observation [*Lennartsson and Shelley*, 1986] suggests a quiet time plasma sheet O^+ density of >0.03 cm^{-3} near solar maximum. This corresponds to a plasma sheet O^+ mass content of ~3000 kg. Using AMPTE data *Greenspan and Hamilton* [2000] reported a ratio of total ring current energy to Dst magnitude of approximately $\sim 2 \times 10^{29}$ keV/nT. Using a quiet time Dst value of −25 nT, an O^+/H^+ ring current ion density ratio of 0.3 by assuming the observed ratio [*Daglis et al.*, 1993] to have the same solar maximum to minimum ratio (~5) as energetic upflowing O^+ ion flux [*Yau et al.*, 1988]), and an averaged energy of 100 keV, the estimated O^+ mass content in the ring current is ~380 kg near solar maximum.

[79] In comparison, as discussed in section 1, the density of O^+ polar wind is seasonally dependent and is on the order of a few to ~30 cm^{-3} near solar maximum. Assuming a seasonally averaged density of 10 cm^{-3}, a K_P-averaged parallel ion velocity of 3 km/s, and an averaged un-trapped ion percentage of 25% reaching the plasma sheet (from Table 1), the flux of un-trapped O^+ ions reaching the plasma sheet is $\sim 7.5 \times 10^5$ cm^{-2} s^{-1}. Assuming uniform polar wind density poleward of 70° invariant, the total area of polar-wind flux tubes at 7000 km altitude in both hemispheres is 2.95×10^{18} cm^2 in the dipole approximation [*Yau et al.*, 1988] and this corresponds to a total rate of $\sim 2.2 \times 10^{24}$ un-trapped O^+ ions s^{-1} and a mass injection rate of ~200 kg/h into the plasma sheet. For an estimated O^+ ring current mass content of ~380 kg, this suggests a filling time of ~4 h.

[80] In summary the simulations and analysis presented show that centrifugal acceleration at higher altitudes (above ~3 R_E altitude) energizes a significant fraction of thermal O^+ to escape velocity and that the fraction of this population reaching the plasma sheet is a factor of ~3 larger in the dusk sector on average compared with the dawn sector. Our results are consistent with the picture that low-energy ion flow constitutes a significant "in-transit" oxygen ion population over a period of a few (~4) hours preceding a magnetic storm, which explains the presence of O^+ ions in the ring current shortly after the onset of the main phase of the storm, when the heavy ions could potentially modify the evolution of the ring current.

[81] **Acknowledgments.** The authors gratefully acknowledge the support of the Canadian Space Agency and the Natural Science and Engineering Research Council (NSERC) Industrial Research Chair Program for this research. W.K.P. was supported by NASA grant NNX12AD25G.

[82] Robert Lysak thanks Charles Chappell and another reviewer for their assistance in evaluating this paper.

References

Abe, T., A. W. Yau, S. Watanabe, M. Yamada, and E. Sagawa (2004), Long-term variation of the polar wind velocity and its implication for the ion acceleration process: Akebono/suprathermal ion mass spectrometer observations, *J. Geophys. Res.*, *109*, A09305, doi:10.1029/2003JA010223.

Chappell, C. R., T. E. Moore, and J. H. Waite Jr. (1987), The ionosphere as a fully adequate source of plasma for the Earth's magnetosphere, *J. Geophys. Res.*, *92*(A6), 5896–5910, doi:10.1029/JA092iA06p05896.

Cladis, J. B. (1986), Parallel acceleration and transport of ions from the polar ionosphere to the plasmasheet, *Geophys. Res. Lett.*, *13*, 893–896, doi:10.1029/GL013i009p00893.

Cully, C. M., E. F. Donovan, A. W. Yau, and G. G. Arkos (2003a), Akebono suprathermal mass spectrometer observations of low-energy ion outflow: Dependence on magnetic activity and solar wind conditions, *J. Geophys. Res.*, *108*(A2), 1093, doi:10.1029/2001JA009200.

Cully, C. M., E. F. Donovan, A. W. Yau, and H. J. Opgenoorth (2003b), Supply of thermal ionospheric ions to the central plasma sheet, *J. Geophys. Res.*, *108*(A2), 1092, doi:10.1029/2002JA009457.

Daglis, I. A., E. T. Sarris, and B. Wilken (1993), AMPTE/CCE CHEM observations of the energetic ion population at geosynchronous altitudes, *Ann. Geophys.*, *11*, 685–696.

Delcourt, D. C., C. R. Chappell, T. E. Moore, and J. H. Waite Jr. (1989), A three dimensional numerical model of ionospheric plasma in the magnetosphere, *J. Geophys. Res.*, *94*, 11,893–11,920, doi:10.1029/JA094iA09p11893.

Delcourt, D. C., J. A. Sauvaud, and T. E. Moore (1993), Polar wind ion dynamics in the magnetotail, *J. Geophys. Res.*, *98*, 9155–9169, doi:10.1029/93JA00301.

Delcourt, D. C., T. E. Moore, and C. R. Chappell (1994), Contribution of low-energy ionospheric protons to the plasma sheet, *J. Geophys. Res.*, *99*, 5681–5689, doi:10.1029/93JA02770.

Drakou, E., A. W. Yau, and T. Abe (1997), Ion temperature measurements from the Akebono suprathermal mass spectrometer: Application to the polar wind, *J. Geophys. Res.*, *102*, 17,523–17,539, doi:10.1029/97JA00099.

Ebihara, Y., M. Yamada, S. Watanabe, and M. Ejiri (2006), Fate of outflowing suprathermal oxygen ions that originate in the polar ionosphere, *J. Geophys. Res.*, *111*, A04219, doi:10.1029/2005JA011403.

Eriksson, A. I., et al. (2006), Electric field measurements on Cluster: Comparing double-probe and electron drift techniques, *Ann. Geophys.*, *24*, 275–289, doi:10.5194/angeo-24-275-2006.

Finlay, C. C., et al. (2010), International Geomagnetic Reference Field: The eleventh generation, *Geophys. J. Int.*, *183*, 1216–1230, doi:10.1111/j.1365-246X.2010.04804.x.

Fok, M. C., R. A. Wolf, R. W. Spiro, and T. E. Moore (2001), Comprehensive computational model of Earth's ring current, *J. Geophys. Res.*, *106*, 8417–8424, doi:10.1029/2000JA000235.

Greenspan, M. E., and D. C. Hamilton (2000), A test of the Dessler-Parker-Sckopke relation during magnetic storms, *J. Geophys. Res.*, *105*, 5419–5430, doi:10.1029/1999JA000284.

Howarth, A., and A. W. Yau (2008), The effects of IMF and convection on thermal ion outflow in magnetosphere-ionosphere coupling, *J. Atmos. Sol. Terr. Phys.*, *70*, 2132–2143, doi:10.1016/j.jastp.2008.08.008.

Huddleston, M. M., C. R. Chappell, D. C. Delcourt, T. E. Moore, B. L. Giles, and M. O. Chandler (2005), An examination of the process and magnitude of ionospheric plasma supply to the magnetosphere, *J. Geophys. Res.*, *110*, A12202, doi:10.1029/2004JA010401.

Hultqvist, B., M. Øieroset, G. Passman, and R. Treuman (Eds.) (1999), *Magnetospheric Plasma Sources and Losses*, Kluwer Acad., Dordrecht, Netherlands, doi:10.1007/978-94-011-4477-3.

Jordanova, V. K. (2003), New insights on geomagnetic storms from model simulations using multi-spacecraft data, *Space Sci. Rev.*, *107*, 157–165, doi:10.1023/A:1025575807139.

Kistler, L. M., et al. (2005), Contribution of nonadiabatic ions to the cross-tail current in an O^+ dominated thin current sheet, *J. Geophys. Res.*, *110*, A06213, doi:10.1029/2004JA010653.

Kistler, L. M., et al. (2006), Ion composition and pressure changes in storm time and nonstorm substorms in the vicinity of the near-Earth neutral line, *J. Geophys. Res.*, *111*, A11222, doi:10.1029/2006JA011939.

Kitamura, N., A. Shinbori, Y. Nishimura, T. Ono, M. Iizima, and A. Kumamoto (2009), Seasonal variations of the electron density distribution in the polar region during geomagnetically quiet periods near solar maximum, *J. Geophys. Res.*, *114*, A01206, doi:10.1029/2008JA013288.

Kitamura, N., et al. (2010), Observations of very-low-energy (<10 eV) ion outflows dominated by O^+ ions in the region of enhanced electron density in the polar cap magnetosphere during geomagnetic storms, *J. Geophys. Res.*, *115*, A00J06, doi:10.1029/2010JA015601.

Lennartsson, O. W., H. L. Collin, and W. K. Peterson (2004), Solar wind control of Earth's H^+ and O^+ outflow rates in the 15-eV to 33-keV energy range, *J. Geophys. Res.*, *109*, A12212, doi:10.1029/2004JA010690.

Lennartsson, W., and E. G. Shelley (1986), Survey of 0.1- to 16-keV/*e* plasma sheet ion composition, *J. Geophys. Res.*, *91*(A3), 3061–3076, doi:10.1029/JA091iA03p03061.

Nilsson, H., et al. (2008), An assessment of the role of the centrifugal acceleration mechanism in high altitude polar cap oxygen ion outflow, *Ann. Geophys.*, *26*, 145–157, doi:10.5194/angeo-26-145-2008.

Northrop, T. G. (1963), *The Adiabatic Motion of Charged Particles*, Wiley-Interscience, New York.

Peterson, W. K., L. Andersson, B. C. Callahan, H. L. Collin, J. D. Scudder, and A. W. Yau (2008), Solar-minimum quiet time ion energization and outflow in dynamic boundary related coordinates, *J. Geophys. Res.*, *113*, A07222, doi:10.1029/2008JA013059.

Peterson, W. K., L. Andersson, B. Callahan, S. R. Elkington, R. W. Winglee, J. D. Scudder, and H. L. Collin (2009), Geomagnetic activity dependence of O^+ in transit from the ionosphere, *J. Atmos. Sol. Terr. Phys.*, *71*, 1623–1629, doi:10.1016/j.jastp.2008.11.003.

Pollock, C. J., M. O. Chandler, T. E. Moore, J. H. Waite Jr., C. R. Chappell, and D. A. Gurnett (1990), A survey of upwelling ion event characteristics, *J. Geophys. Res.*, *95*, 18,969–18,980, doi:10.1029/JA095iA11p18969.

Ruohoniemi, J. M., and R. A. Greenwald (1996), Statistical patterns of high-latitude convection obtained from Goose Bay HF radar observations, *J. Geophys. Res.*, *101*, 21,743–21,763, doi:10.1029/96JA01584.

Seki, K., et al. (2003), Cold ions in the hot plasma sheet of Earth's magnetotail, *Nature*, *422*, 589–592, doi:10.1038/nature01502.

Shepherd, S. G., and J. M. Ruohoniemi (2000), Electrostatic potential patterns in the high-latitude ionosphere constrained by SuperDARN measurements, *J. Geophys. Res.*, *105*, 23,005–23,014, doi:10.1029/2000JA000171.

Su, Y. J., J. L. Horwitz, T. E. Moore, B. L. Giles, M. O. Chandler, P. D. Craven, M. Hirahara, and C. J. Pollock (1998), Polar wind survey with the thermal ion dynamics experiment/plasma source instrument suite aboard POLAR, *J. Geophys. Res.*, *103*, 29,305–29,337, doi:10.1029/98JA02662.

Sugiura, M., and D. J. Poros (1971), Hourly values of equatorial *Dst* for years 1957 to 1970, *Rep. X-645-71-278*, NASA Goddard Space Flight Cent., Greenbelt, Md.

Tsyganenko, N. A. (1989), A magnetospheric magnetic field model with a warped tail current sheet, *Planet. Space Sci.*, *37*, 5–20, doi:10.1016/0032-0633(89)90066-4.

Tsyganenko, N. A. (1995), Modeling the Earth's magnetospheric magnetic field confined within a realistic magnetopause, *J. Geophys. Res.*, *100*, 5599–5612, doi:10.1029/94JA03193.

Tsyganenko, N. A., and D. P. Stern (1996), Modeling the global magnetic field of the large-scale Birkeland current systems, *J. Geophys. Res.*, *101*, 27,187–27,198, doi:10.1029/96JA02735.

Watanabe, S., B. A. Whalen, and A. W. Yau (1992), Thermal ion observations of depletion and refilling in the plasmaspheric trough, *J. Geophys. Res.*, *97*, 1081–1096, doi:10.1029/91JA02818.

Weimer, D. R. (2001), An improved model of ionospheric electric potentials including substorm perturbations and application to the Geospace Environment Modeling November 24, 1996, event, *J. Geophys. Res.*, *106*, 407–416, doi:10.1029/2000JA000604.

Yau, A. W., and M. Andre (1997), Source processes in the high latitude ionosphere, *Space Sci. Rev.*, *80*, 1–25, doi:10.1023/A:1004947203046.

Yau, A. W., E. G. Shelley, W. K. Peterson, and L. Lenchyshyn (1985), Energetic auroral and polar ion outflow at DE-1 altitudes: Magnitude, composition, magnetic activity dependence, and long-term variations, *J. Geophys. Res.*, *90*, 8417–8432, doi:10.1029/JA090iA09p08417.

Yau, A. W., W. K. Peterson, and E. G. Shelley (1988), Quantitative parameterization of energetic ionospheric ion outflow, in *Modeling Magnetospheric Plasma*, *Geophys. Monogr. Ser.*, vol. 44, edited by T. E. Moore et al., pp. 211–217, AGU, Washington, D. C., doi:10.1029/GM044p0211.

Yau, A. W., B. A. Whalen, and E. Sagawa (1991), Minor ion composition in the polar ionosphere, *Geophys. Res. Lett.*, *18*, 345–348, doi:10.1029/91GL00034.

Yau, A. W., T. Abe, and W. K. Peterson (2007), The polar wind: Recent observations, *J. Atmos. Sol. Terr. Phys.*, *69*, 1936–1983, doi:10.1016/j.jastp.2007.08.010.

Zaharia, S., V. K. Jordanova, M. F. Thomsen, and G. D. Reeves (2006), Self-consistent modeling of magnetic fields and plasmas in the inner magnetosphere: Application to a geomagnetic storm, *J. Geophys. Res.*, *111*, A11S14, doi:10.1029/2006JA011619.